drhein-Westfalen. The computer time was generously provided by the Rechenzentrum der Universität Bielefeld and by the Rechenzentrum der Universität Köln. Some of the calculations were also carried out at the Interdata 8/32 minicomputer (Universität Bochum), sponsored by the Deutsche Forschungsgemeinschaft. We also thank Professor V. Staemmler for interesting discussions and valuable suggestions and the reviewers for useful comments.

Registry No. **1** (X = H), 51272-82-3; **1** (X = H), radical cation, 86834-53-9; **1** (X = NH_2), 86834-48-2; **1** (X = CH_2^-·), 86834-49-3; **1** (X = BH_2), 86834-50-6; **1** (X = CH_2^+·), 86834-51-7; **4**, 86834-52-8; diphosphaethylene, 41916-72-7.

Contribution from the Department of Chemistry,
Texas A&M University, College Station, Texas 77843

Electronic Structure of Metal Clusters. 4. Photoelectron Spectra and Molecular Orbital Calculations on Cobalt, Iron, Ruthenium, and Osmium Sulfide Nonacarbonyl Clusters

PETER T. CHESKY and MICHAEL B. HALL*

Received January 31, 1983

Gas-phase, ultraviolet photoelectron (PE) spectra and molecular orbital (MO) calculations are reported for $SCo_3(CO)_9$, $SH_{n-1}Fe_nCo_{3-n}(CO)_9$ (n = 1-3), $S_2Fe_3(CO)_9$, and $SH_2M_3(CO)_9$ (M = Fe, Ru, Os). The first PE spectra reported for mixed-metal clusters are included in this series. As Co atoms are replaced by the isoelectronic FeH unit, the spectra show the loss of a Co band and the appearance of an Fe band. This phenomenon suggests that the d bands localize upon ionization. In a comparison with the PE spectrum of $M_3(CO)_{12}$ (M = Fe, Ru, Os), the major spectral changes for $SH_2M_3(CO)_9$ (M = Fe, Ru, Os) are the loss of a band corresponding to direct M-M interactions and the appearance of bands due to a mixture of energy-equivalent M-H-M and M-S interactions. The spectra also show a substantial rearrangement of the bands due to the t_{2g}-like electrons, which are usually considered M-CO π bonding. An antibonding interaction between a S orbital and the t_{2g}-like orbitals is responsible for a unique band in the spectra which occurs at high ionization energy between the M-M bonding band and the main t_{2g}-like band.

Introduction

Metal-sulfur clusters are interesting because of their implication in poisoning of catalysts by sulfur and as models for hydrodesulfurization catalysts.[1] The systematic investigation of $Co_2(CO)_8$-catalyzed hydroformylations with olefinic compounds and sulfur impurities resulted in the identification of various cobalt and cobalt carbonyl sulfides including $SCo_3(CO)_9$.[2] While studying the reaction of synthesis gas with thiophene in the presence of $Co_2(CO)_8$ and $Fe(CO)_5$, Khattab et al. isolated $SFeCo_2(CO)_9$. This mixed-metal cluster was among the first carbonyl compounds containing a metal-metal bond between two different transition-metal atoms and the first mixed-metal sulfide carbonyl cluster.[3] The advances in the field of transition-metal cluster chemistry in the past decade are evident by the numerous reviews discussing the preparation of new cluster compounds of increasing nuclearity and complexity.[4] These compounds are of additional interest because of the similarities between chemisorption on transition-metal surfaces and the chemistry of conventional transition-metal clusters.[5] Despite the early synthesis and novelty of these sulfide carbonyl clusters, their chemistry has not been as thoroughly investigated as the isostructural $RCCo_3(CO)_9$ clusters.[6]

The crystal structure of $SCo_3(CO)_9$ confirmed that the molecular geometry consists of a triangle of cobalt tricarbonyl fragments capped by a S atom.[7] The X-ray structure determination of $SFeCo_2(CO)_9$ (**1**) showed it to be isomorphous

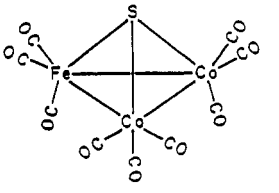

1

with $SCo_3(CO)_9$.[8] The sulfur atom in the paramagnetic $SCo_3(CO)_9$ cluster contributes four electrons to the $Co_3(CO)_9$

(1) (a) Burke, D. P. *Chem. Week* **1979**, 46. (b) Marko, L. *Gazz. Chim. Ital.* **1979**, *109*, 247. (c) Satterfield, C. N. *CHEMTECH* **1981**, 618.
(2) (a) Greenfield, H.; Metlin, S.; Orchin, M.; Wender, I. *J. Org. Chem.* **1958**, *23*, 1054. (b) Marko, L.; Bor, G.; Klumpp, E. *Chem. Ind. (London)* **1961**, 1491. (c) Marko, L.; Bor, G.; Almasy, G. *Chem. Ber.* **1961**, *94*, 847. (d) Marko, L.; Bor, G.; Klumpp, E.; Marko, B.; Almasy, G. *Ibid.* **1963**, *96*, 955. (e) Marko, L.; Bor, G.; Klumpp, E. *Angew. Chem.* **1963**, *75*, 248. (f) Klumpp, E.; Bor, G.; Marko, L. *Chem. Ber.* **1967**, *100*, 1451.
(3) Khattab, S. A.; Marko, L.; Bor, G.; Marko, B. *J. Organomet. Chem.* **1964**, *1*, 373.
(4) (a) Abel, E. W.; Stone, F. G. A. *Q. Rev., Chem. Soc.* **1969**, *23*, 325. (b) Johnston, R. D. *Adv. Inorg. Chem. Radiochem.* **1970**, *13*, 471. (c) King, R. B. *Prog. Inorg. Chem.* **1972**, *15*, 287. (d) Lewis, J.; Johnson, B. F. G. *Pure Appl. Chem.* **1975**, *44*, 43. (e) Wade, K. *Adv. Inorg. Chem. Radiochem.* **1976**, *18*, 1. (f) Chini, P.; Longoni, G.; Albano, V. G. *Adv. Organomet. Chem.* **1976**, *14*, 285. (g) Chini, P.; Heaton, B. T. *Top. Curr. Chem.* **1977**, *71*, 1. (h) Vahrenkamp, H. *Struct. Bonding (Berlin)* **1977**, *32*, 11. (i) Schmid, G. *Angew. Chem., Int. Ed. Engl.* **1978**, *17*, 392. (j) Gladfelter, W. L.; Geoffroy, G. L. *Adv. Organomet. Chem.* **1980**, *1*, 207. (k) Johnson, B. F. G.; Lewis, J. *Adv. Inorg. Chem. Radiochem.* **1981**, *24*, 225. (l) Manning, M. C.; Trogler, W. C. *Coord. Chem. Rev.* **1981**, *38*, 89.
(5) (a) Tolman, C. A. *Chem. Soc. Rev.* **1972**, *1*, 337. (b) Ugo, R. *Catal. Rev.—Sci. Eng.* **1975**, *11*, 225. (c) Muetterties, E. L. *Bull. Soc. Chim. Belg.* **1975**, *84*, 959. (d) Muetterties, E. L. *Ibid.* **1976**, *85*, 451. (e) Muetterties, E. L.; Rhodin, T. N.; Band, E.; Brucker, C. F.; Pretzer, W. R. *Chem. Rev.* **1979**, *79*, 91. (f) Chini, P. *Gazz. Chim. Ital.* **1979**, *109*, 225. (g) Ertl, G. *Ibid.* **1979**, *109*, 217. (h) Muetterties, E. L. *Isr. J. Chem.* **1980**, *20*, 84. (i) Evans, J. *Chem. Soc. Rev.* **1981**, *10*, 159. (j) Muetterties, E. L. *Catal. Rev.—Sci. Eng.* **1981**, *23*, 69. (k) Muetterties, E. L. *Inorg. Chim. Acta* **1981**, *50*, 1.
(6) (a) Palyi, G.; Placenti, F.; Marko, L. *Inorg. Chim. Acta, Rev.* **1970**, *4*, 109. (b) Penfold, B. R.; Robinson, B. H. *Acc. Chem. Res.* **1973**, *6*, 73. (c) Seyferth, D. *Adv. Organomet. Chem.* **1976**, *14*, 97. (d) Schmid, G. *Angew. Chem., Int. Ed. Engl.* **1978**, *17*, 392. (e) Schmid, G. *Angew. Chem.* **1978**, *90*, 417.
(7) Wei, C. H.; Dahl, L. F. *Inorg. Chem.* **1967**, *6*, 1229.
(8) Stevenson, D.; Wei, C. H.; Dahl, L. F. *J. Am. Chem. Soc.* **1971**, *93*, 6027.

0020-1669/83/1322-2998$01.50/0

fragment, one electron in excess of the "closed shell" configuration. The diamagnetic $SFeCo_2(CO)_9$ cluster is isoelectronic with the oxidized cation of $SCo_3(CO)_9$ since removing the unpaired electron is equivalent to the replacement of an Co atom with an Fe atom. Since the metal–metal bond lengths were 0.083 Å shorter in $SFeCo_2(CO)_9$ than in $SCo_3(CO)_9$, Dahl et al. suggested that the molecular orbital containing the unpaired electron in $SCo_3(CO)_9$ must be composed of antibonding metal–metal interactions. An approximate force field calculation, derived from M–S stretching modes of μ_3-bridging S atoms in metal clusters, showed almost identical M–S bond strengths but stronger M–M bonds in $SFeCo_2(CO)_9$ than in $SCo_3(CO)_9$.[9]

The ESR hyperfine parameters of $SCo_3(CO)_9$ revealed that the molecular orbital containing the unpaired electron is an antibonding orbital of a_2 symmetry. This orbital consists primarily of cobalt d_{xz} atomic orbitals localized in the tricobalt basal plane.[10] The lack of the bridging atom's interaction with the basal metal plane was verified by the negligible change in the hyperfine parameters of the ESR spectrum for $SeCo_3(CO)_9$.[11] Electrochemical studies on $SFeCo_2(CO)_9$ showed a reversible one-electron reduction to the radical anion. The half-life of the $SFeCo_2(CO)_9$ radical anion is a small fraction of the more stable $RCCo_3(CO)_9$ radical anion. The second one-electron reduction of $SFeCo_2(CO)_9$ is an irreversible process probably due to fragmentation.[12]

An excellent qualitative discussion of the bonding in these and related clusters has been provided by the recent work of Schilling and Hoffmann.[13] More recently Fenske et al. performed Fenske–Hall molecular orbital (MO)[14] calculations on $S_2Fe_3(CO)_9$ and related compounds. They also employed an empirical molecular orbital localization parameter to identify whether the orbitals are bonds or lone pairs.[15] Nevertheless, there remain questions of a more quantitative nature about the ordering of one-electron orbitals, the overall charge distribution, differences in mixed metal–metal and metal–sulfur bonding, and the effects of bridging hydrogen atoms on the basal metal–metal bonds.

This study will examine the bonding in the $SH_{n-1}Fe_nCo_{3-n}(CO)_9$ (n = 1–3) series, $S_2Fe_3(CO)_9$, $SH_2Ru_3(CO)_9$, and $SH_2Os_3(CO)_9$, using gas-phase, ultraviolet photoelectron (PE) spectroscopy. The PE spectra will be interpreted by observing trends within the series and comparing the spectra with parameter-free molecular orbital calculations. We have previously investigated the electronic structures of similar clusters, $(\mu_3\text{-CR})Co_3(CO)_9$[16a] and $(\mu_3\text{-CR})H_3Ru_3(CO)_9$,[16b] by means of PE spectroscopy and MO calculations. It was possible to assign the ionization bands and to quantitatively discuss the bonding in all compounds. A preliminary report of the mixed-metal sulfides has appeared.[17]

Experimental and Theoretical Section

Preparation. The preparation and purification of $SCo_3(CO)_9$,[2f] $SFeCo_2(CO)_9$,[3] $SHFe_2Co(CO)_9$,[18] $SH_2Fe_3(CO_9$,[19] $S_2Fe_3(CO)_9$,[20] $SH_2Ru_3(CO)_9$,[21] and $SH_2Os_3(CO)_9$[21b] are from published procedures.

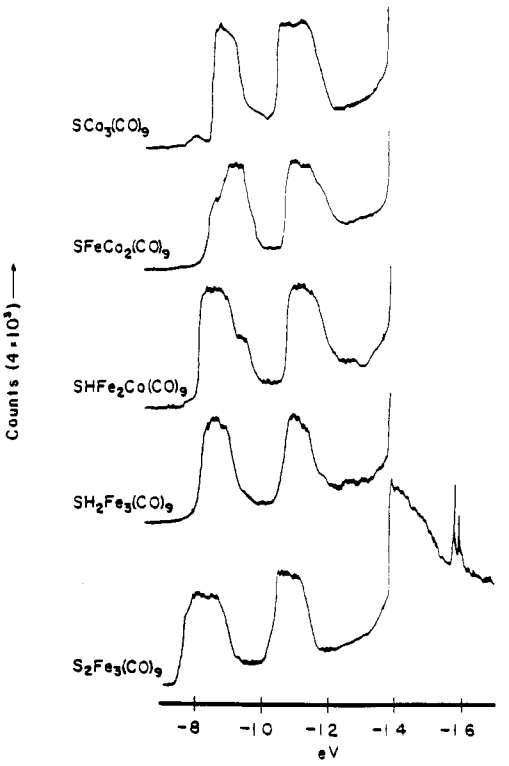

Figure 1. Partial photoelectron spectra of $SCo_3(CO)_9$, the isoelectronic series $SH_{n-1}Fe_nCo_{3-n}(CO)_9$ (n = 1–3), and $S_2Fe_3(CO)_9$.

Spectroscopy. The He I ultraviolet photoelectron spectra were recorded on a Perkin-Elmer Model PS-18 spectrometer. The total spectrum was recordied as a single slow scan with the argon $^2P_{3/2}$ and $^2P_{1/2}$ lines at 15.76 and 15.94 eV used as the internal reference. The resolution for all spectra was better than 30 meV for the fwhm of the Ar $^3P_{1/2}$ peak. Since no free-CO spike at 14 eV was noted, all compounds were stable and did not decompose in the spectrometer.

Theoretical Procedure. The Fenske–Hall molecular orbital calculations, a nonempirical, self-consistent-field procedure, were performed on an Amdahl 470 V/6 computer. The method has no adjustable parameters, and the results depend totally on the basis set and the molecular geometry.[14] The Co, Fe, and Ru basis functions (1s through nd) were taken from Richardson et al.[22] and were augmented by $(n + 1)$s and $(n + 1)$p functions with exponents of 2.0 for Fe and Co and 2.2 for Ru. The carbon, oxygen, and sulfur functions were taken from the double-ζ functions of Clementi[23] and reduced to a single-ζ function,[24] except for the p valence functions, which were retained as the double-ζ function. An exponent of 1.2 was used for the hydrogen atoms. Mulliken population analysis was used to determine both the individual atomic charges and the atomic orbital populations. Overlap populations between atoms were calculated and used to predict trends in the bond strength.

The molecular geometry of the $SH_{n-1}Fe_nCo_{3-n}(CO)_9$ (n = 1–3) series was taken from the $SCo_3(CO)_9$ crystal structure[7] and frozen in order to study the effect of mixed metal–metal and metal–hydrogen–metal interactions without superimposing additional geometric changes. The hydrogen atoms for $SHFe_2Co(CO)_9$ and $SH_2Fe_3(CO)_9$

(9) (a) Oxton, I. A.; Powell, D. B.; Skinner, P.; Marko, L.; Werner, H. *Inorg. Chim. Acta* **1981**, *47*, 177. (b) Hempleman, A. J.; Oxton, I. A.; Powell, D. B.; Skinner, P.; Deeming, A. J.; Marko, L. *J. Chem. Soc., Faraday Trans. 2* **1981**, *77*, 1669.
(10) Strouse, C. E.; Dahl, L. F. *Discuss. Faraday Soc.* **1969**, *47*, 93.
(11) Strouse, C. E.; Dahl, L. F. *J. Am. Chem. Soc.* **1971**, *93*, 6032.
(12) Peake, B. M.; Rieger, P. H.; Robinson, B. H.; Simpson, J. *Inorg. Chem.* **1981**, *20*, 2540.
(13) (a) Shilling, B. E.; Hoffmann, R. *J. Am. Chem. Soc.* **1978**, *100*, 6274. (b) *Ibid.* **1979**, *101*, 3456.
(14) Hall, M. B.; Fenske, R. F. *Inorg. Chem.* **1972**, *11*, 768.
(15) Rives, A. B.; Xiao-Zeng, Y.; Fenske, R. F. *Inorg. Chem.* **1982**, *21*, 2286.
(16) (a) Part 1: Chesky, P. T.; Hall, M. B. *Inorg. Chem.* **1981**, *20*, 4419. (b) Part 3: Sherwood, D. E., Jr.; Hall, M. B. *Organometallics* **1982**, *1*, 1519.
(17) (a) Presented in part at the 37th Southwest Regional Meeting of the American Chemical Society, San Antonio, TX, Dec 9–11, 1981; Abstract 76. (b) Chesky, P. T.; Hall, M. B. *Inorg. Chem.* **1983**, *22*, 2102.
(18) Marko, L. *J. Organomet. Chem.* **1981**, *213*, 271.
(19) Marko, L.; Takacs, J.; Papp, S.; Marko-Monostory, B. *Inorg. Chim. Acta* **1980**, *45*, L189.
(20) Hieber, W.; Gruber, J. *Z. Anorg. Allg. Chem.* **1958**, *296*, 91.
(21) (a) Deeming, A. J.; Ettorre, R.; Johnson, B. F. G.; Lewis, J. *J. Chem. Soc. A* **1971**, 1797. (b) Deeming, A. J.; Underhill, M. *J. Organomet. Chem.* **1972**, *42*, C60. (c) Sappa, E.; Gambino, O.; Cetini, G. *Ibid.* **1972**, *35*, 375. (d) Cresswell, T. A.; Howard, J. A. K.; Kennedy, F. G.; Knox, S. A. R.; Wadepohl, H. *J. Chem. Soc., Dalton Trans.* **1981**, *11*, 2220.
(22) (a) Richardson, J. W.; Nieuwpoort, W. C.; Powell, R. R.; Edgell, W. F. *J. Chem. Phys.* **1962**, *44*, 1344. (b) Richardson, J. W.; Blackman, M. J.; Ranochak, J. E. *J. Chem. Phys.* **1973**, *58*, 3010.
(23) (a) Clementi, E. *J. Chem. Phys.* **1964**, *40*, 1944. (b) Clementi, E. *IBM J. Res. Dev.* **1965**, *9*, 2.
(24) Fenske, R. F.; Radtke, D. D. *Inorg. Chem.* **1968**, *7*, 479.

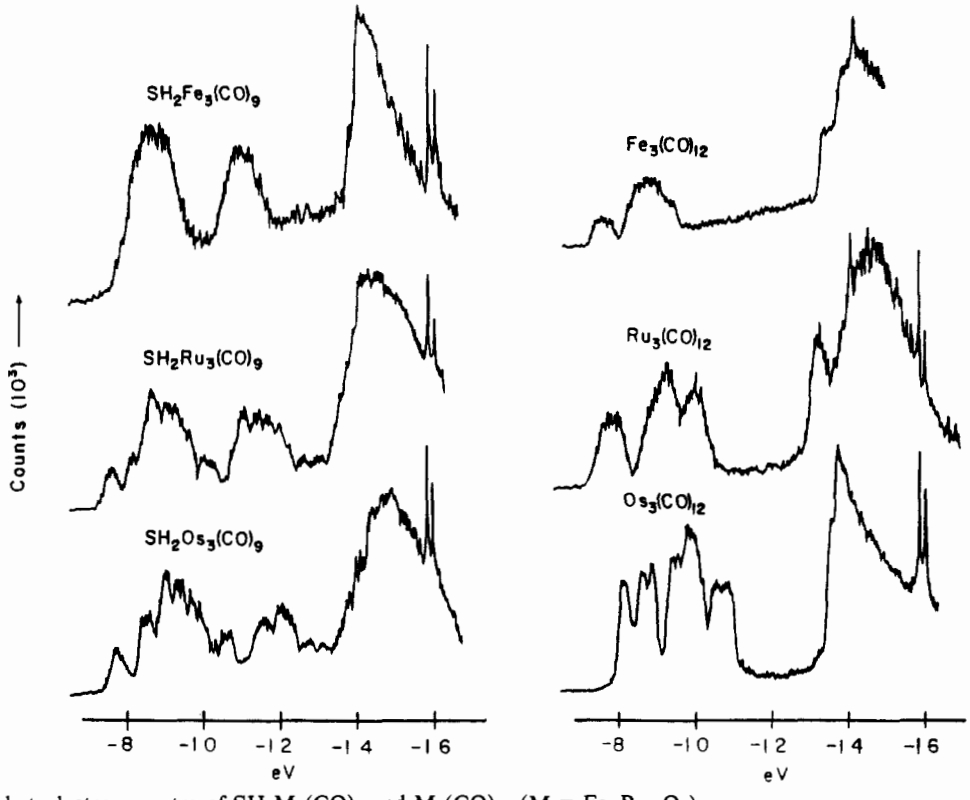

Figure 2. Partial photoelectron spectra of $SH_2M_3(CO)_9$ and $M_3(CO)_{12}$ (M = Fe, Ru, Os).

Table I. Absolute Values for PES Ionization Peak Maxima (eV) in $SCo_3(CO)_9$, $SH_{n-1}Fe_nCo_{3-n}(CO)_9$ (n = 1-3), and $S_2Fe_3(CO)_9$[a]

band	$SCo_3(CO)_9$	$SFeCo_2(CO)_9$	$SHFe_2Co(CO)_9$	$SH_2Fe_3(CO)_9$	$S_2Fe_3(CO)_9$
1	8.1 (w)	8.5 (w)	8.4	8.7	8.1
	8.9	9.1	9.1	9.1	8.5
	9.1	9.4	9.5 (w)		8.7
2	10.8	10.9	11.0	11.0	10.6
	11.3	11.2	11.2	11.2	11.0
3			12.3 (vw)	12.3 (vw)	
				13.2 (vw)	

[a] Abbreviations: vw = very weak intensity; w = weak intensity.

Table II. Absolute Values for PES Ionization Peak Maxima (eV) in $SH_2M_3(CO)_9$ (M = Ru, Os)[a]

band	$SH_2Ru_3(CO)_9$	$SH_2Os_3(CO)_9$	band	$SH_2Ru_3(CO)_9$	$SH_2Os_3(CO)_9$
1	7.5 (w)	7.7 (w)	2	11.0	11.7
	8.1 (w)	8.5 (w)		11.4	12.1
	8.6	9.0		11.8	12.2
	9.0	9.3	3	12.4 (vw)	12.7 (vw)
	9.2	9.4		13.1 (vw)	13.3 (vw)
	9.4	9.6			
	9.6	9.9			
	10.0 (w)	10.6 (w)			

[a] Abbreviations: vw = very weak intensity; w = weak intensity.

were placed in the M-S-M plane, below the basal metal plane, at normal Fe-H distances.[25] The orientations of the carbonyls were shifted slightly such that the $M(CO)_3$ geometry was pseudooctahedral. The exact molecular structure of $S_2Fe_3(CO)_9$[26] and the structure values for $SH_2Ru_3(CO)_9$[27] averaged with those of $SH_2Os_3(CO)_9$[28] were used for these calculations.

Results

Photoelectron Spectra. The ionization energy (IE) range of interest spans 7-14 eV. The IE region above 14 eV will not be discussed because of the normally broad and poorly resolved bands due to carbonyl 5σ and 1π ionizations. Each spectrum contains two predominant bands occurring below 14 eV. The shape of the low-IE band is dependent upon the Co/Fe ratio, and the number of resolved peaks increases from Fe to Ru to Os.

The low-IE photoelectron spectra for $SCo_3(CO)_9$, $SFeCo_2(CO)_9$, $SHFe_2Co(CO)_9$, $SH_2Fe_3(CO)_9$, and $S_2Fe_3(CO)_9$ are shown in Figure 1. Table I lists the IE maxima for these clusters. Only the $SCo_3(CO)_9$ spectrum shows a low-energy, low-intensity peak occurring before the onset of the high-intensity bands located at 9 eV. In the $SFeCo_2(CO)_9$, $SHFe_2Co(CO)_9$, and $SH_2Fe_3(CO)_9$ spectra the shape of the first band reflects the varying Fe/Co ratio. As the Fe composition increases, the intensity of the low-energy side increases. Conversely, the intensity of the high-energy portion of the band decreases with increasing Fe content and completely disappears in $SH_2Fe_3(CO)_9$. The spectra for $SHFe_2Co(CO)_9$ and $SH_2Fe_3(CO)_9$ feature additional, weak bands between 12.3 and 13.2 eV. The spectrum for $S_2Fe_3(CO)_9$ displays a broader low-energy band. All clusters have their second intense IE band occurring at about the same energy.

The low-IE photoelectron spectra of $SH_2M_3(CO)_9$ (M = Fe, Ru, Os) and the "parent" carbonyls, $M_3(CO)_{12}$ (M = Fe, Ru, Os), are shown in Figure 2. Table II lists the IE maxima for $SH_2M_3(CO)_9$ (M = Ru, Os). The PE spectrum for both $SH_2Ru_3(CO)_9$ and $SH_2Os_3(CO)_9$ show two weak, low-energy ionizations occurring below 8.6 eV. The next IE band is a manifold of closely spaced peaks. These peaks are more distinctive for the Os analogue. The second IE band for both of these compounds is also a composite of several peaks. Another feature in the $SH_2M_3(CO)_9$ (M = Ru, Os) PE spectra is weak band(s) between 12.0 and 13.3 eV.

Molecular Orbital Calculations: Fragment Analysis. In large molecules the complexity of the MO pattern, caused by a large

(25) Bau, R.; Teller, R. G.; Kirtley, S. W.; Koetzle, T. F. *Acc. Chem. Res.* **1979**, *12*, 176.
(26) Wei. C. H.; Dahl, L. F. *Inorg. Chem.* **1965**, *4*, 493.
(27) Adams, R. D.; Katahira, D. A. *Organometallics* **1982**, *1*, 53.
(28) Johnson, B. F. G.; Lewis, J.; Pippard, D.; Raithby, P. R.; Sheldrick, G. M.; Rouse, K. D. *J. Chem. Soc., Dalton Trans.* **1979**, *9*, 616.

Table III. Atomic Composition of $Co(CO)_3$ Fragments

	% atomic composition				
orbital	3d	4s	4p	CO 5σ	CO 2π
$6a_1$ (LUMO)	8	9	27	3	52
7e (HOMO)	67		9	7	16
$5a_1$	83			5	7
6e	77		2	5	16

number of closely spaced MO's, becomes difficult to interpret in terms of their atomic components. To simplify this problem, one can analyze the MO's of the molecule in terms of preformed components. One approach is fragment analysis, where one views the sulfide cluster as formed from three $M(CO)_3$ fragments and the capping S atom. This approach has been used successfully to describe the bonding in alkylidyne nonacarbonyl clusters.[16] The numbering of the molecular orbitals of the clusters and fragments begins with the lowest energy valence molecular orbitals, except for the carbonyls, where 1σ and 2σ are O 1s and C 1s, respectively.

$SCo_3(CO)_9$ and $SFeCo_2(CO)_9$. The $Co(CO)_3$ fragments in $SCo_3(CO)_9$ were idealized to C_{3v} symmetry. The lowest lying molecular orbitals of $Co(CO)_3$ consist of symmetry-adapted combinations of carbonyl 3σ, 4σ, and 1π. The next group of orbitals ($4a_1$ and 5e), forming the Co–CO σ bond, show donation from carbonyl 5σ orbitals to the metal orbitals. The 6e and $5a_1$ fragment orbitals occur at much higher energies and are predominantly Co 3d. These orbitals, which are stabilized by carbonyl 2π interactions, correspond to the t_{2g}-like orbitals of an octahedral (O_h) system. The HOMO for $Co(CO)_3$, 7e, consists primarily of Co 3d with some diffuse 4p contributions and corresponds to the e_g-like orbitals of an O_h system. In the neutral $Co(CO)_3$ fragment the 7e orbitals (HOMO) are occupied by three electrons. The $6a_1$ orbital (LUMO) contains more Co diffuse 4p and 4s than compact 3d character. The most important orbitals for the formation of the cluster (6e, $5a_1$, 7e, and $6a_1$) have their atomic character listed in Table III.

We will concentrate on the interaction of $Co(CO)_3$'s higher energy orbitals with S 3p to describe the formation of the $SCo_3(CO)_9$ cluster. Despite the fact that lower energy fragment orbitals may be delocalized over the entire cluster, they do not contribute to cluster formation. The MO diagrams for the formation of $SCo_3(CO)_9$ and $SFeCo_2(CO)_9$ from their fragments are shown in Figure 3.

The HOMO in $SCo_3(CO)_9$ is Co–Co antibonding. This orbital occurs above the more stable $14a_1$ and 20e, which correspond to Co–Co bonding orbitals. The $13a_1$ orbital, which has Co–S antibonding interactions, is repelled by $11a_1$, an orbital of similar, but bonding, character. Occurring just below $13a_1$ are the group of orbitals that represent Co–CO t_{2g}-like interactions. At lower energy are the orbitals that represent Co–S bonding interactions. The compositions of the $SCo_3(CO)_9$ molecular orbitals are summarized in Table IV.

From the fragment analysis it is clear that the $Co(CO)_3$ fragments' 7e and $6a_1$ orbitals are involved in the cluster formation, while $5a_1$ and 6e contribute little to the net bonding. In the free neutral fragments the orbital populations are $6e^{4.0}5a_1^{2.0}7e^{3.0}6a_1^{0.0}$, while the final cluster's populations are $6e^{3.9}5a_1^{2.0}7e^{2.5}6a_1^{0.5}$. The capping S atom's 3p orbitals gain the remainder of the fragments' electron density, and S has a gross charge of 0.13−.

Figure 3 also shows the fragment analysis of $SFeCo_2(CO)_9$. The $Co(CO)_3$ and $Fe(CO)_3$ fragments were idealized to C_{3v} symmetry. The $Fe(CO)_3$ fragment orbitals are almost the same as those of $Co(CO)_3$ but shifted to slightly higher energy. The HOMO, 37a′, for $SFeCo_2(CO)_9$ is metal–metal bonding. The large percent character of Fe 7e and Co $6a_1$ raises the HOMO's energy level to separate it from the other M–M

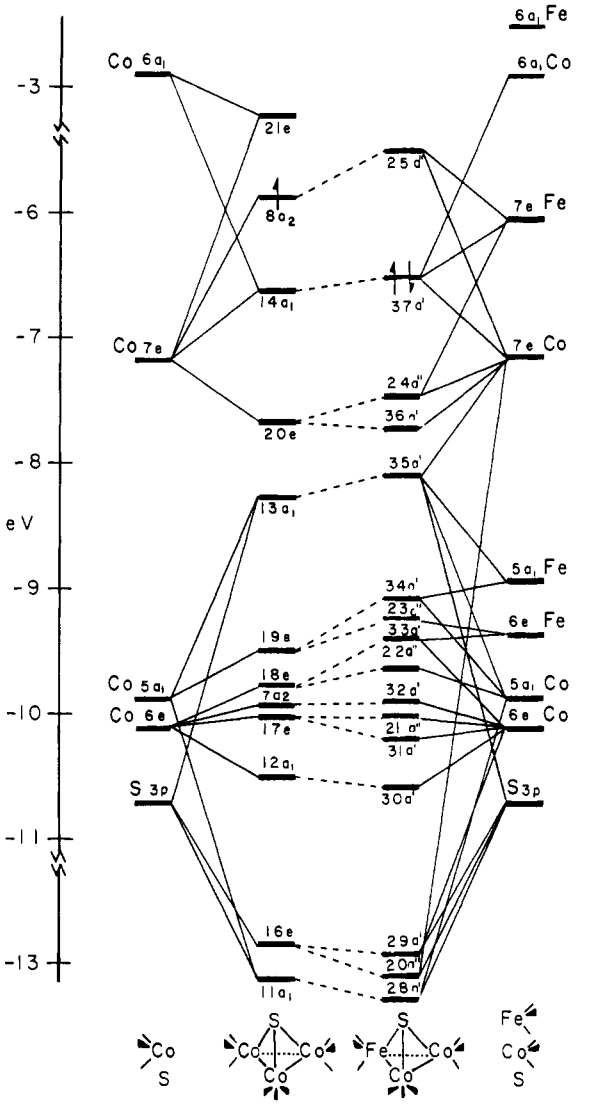

Figure 3. Molecular orbital bonding scheme for $SCo_3(CO)_9$ and $SFeCo_2(CO)_9$. The energy values were obtained from a Fenske–Hall calculation. Connectivity lines indicate the principal contributions to each molecular orbital.

Table IV. Molecular Composition of $SCo_3(CO)_9$

	% fragment composition				
orbital	$6a_1$	7e	$5a_1$	6e	S
21e (LUMO)	20	68			10
$8a_2$ (HOMO)		100			
$14a_1$	23	70	6		
20e	3	95			
$13a_1$	7	16	47	7	22
19e	1	3	89	3	3
18e		9	6	79	5
$7a_2$				100	
17e				100	
$12a_1$			8	90	
16e	8	16	5	17	54
$11a_1$	4		33		62

e_g-like bonding MO's. The 35a′ orbital, identical in character with the $SCo_3(CO)_9$ cluster's $13a_1$, is similarly destabilized by some antibonding M–S character. The M–CO t_{2g}-like orbitals span a larger MO energy range in $SFeCo_2(CO)_9$ than in $SCo_3(CO)_9$ because of the inherent energy gap between Co and Fe fragments' $5a_1$ and 6e. The M–S bonding interactions occur at approximately the same energy for both clusters.

In terms of the fragment analysis both the $Co(CO)_3$ and $Fe(CO)_3$ fragments' 7e and $6a_1$ orbitals are involved in the

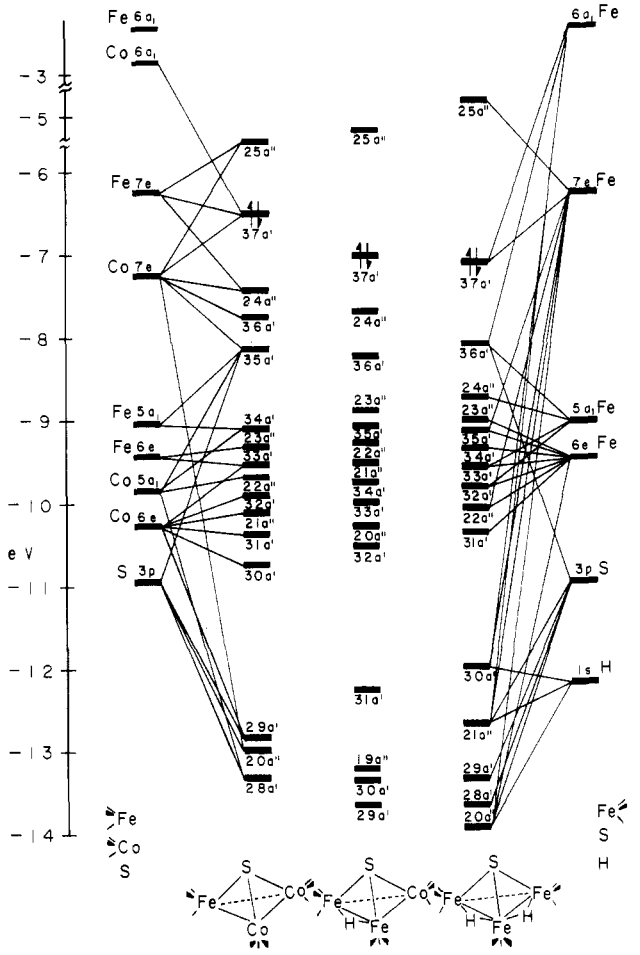

Figure 4. Molecular orbital bonding scheme for the isoelectronic series $SH_{n-1}Fe_nCo_{3-n}(CO)_9$ (n = 1–3). The energy values were obtained from a Fenske–Hall calculation. Connectivity lines indicate the principal contributions to each molecular orbital.

cluster formation. The free neutral fragments' orbital populations are $6e^{4.0}5a_1{}^{2.0}7e^{3.0}6a_1{}^{0.0}$ and $6e^{4.0}5a_1{}^{2.0}7e^{2.0}6a_1{}^{0.0}$ for $Co(CO)_3$ and $Fe(CO)_3$, respectively. The final cluster's populations for $Co(CO)_3$ and $Fe(CO)_3$ are $6e^{3.9}5a_1{}^{2.0}7e^{2.6}6a_1{}^{0.4}$ and $6e^{3.9}5a_1{}^{2.0}7e^{1.6}6a_1{}^{0.4}$, respectively. The capping S atom's 3p orbital also acquires most of the remaining electron density, and S has an overall negative charge of 0.17–.

$SHFe_2Co(CO)_9$ and $SH_2Fe_3(CO)_9$. The important molecular orbitals for the isoelectronic series $SH_{n-1}Fe_nCo_{3-n}(CO)_9$ (n = 1–3) are shown in Figure 4. The $SHFe_2Co(CO)_9$ and $SH_2Fe_3(CO)_9$ clusters have as new features M–H–M interactions. The calculated eigenvalues (orbital energies) for the isoelectronic series produce some interesting trends. The energy gap between the LUMO and HOMO increases as the Fe content increases. As one proceeds from $SFeCo_2(CO)_9$ to $SHFe_2Co(CO)_9$ to $SH_2Fe_3(CO)_9$, the number of M–M bonding orbitals decreases from three (37a′, 24a″, 36a′) to two (37a′, 24a″) to one (37a′), while the number of M–H–M orbitals increases from zero to one (31a′) to two (30a′, 21a″).

The second region of interest is the t_{2g}-like orbitals, which are primarily M–CO bonding. The energy span for these MO's appears to be constant, but the IE's shift to slightly higher energy as the Fe content increases. In all three clusters one of the t_{2g}-like orbitals contains some S and is destabilized to slightly higher energy, filling the e_g–t_{2g} orbital gap. This orbital is 35a′ in $SFeCo_2(CO)_9$ and 36a′ in both $SHFe_2Co(CO)_9$ and $SH_2Fe_3(CO)_9$.

The third region contains S–M interactions. The eigenvalues for these interactions indicate a constant energy span with a slight decrease in absolute value with increasing Fe and H

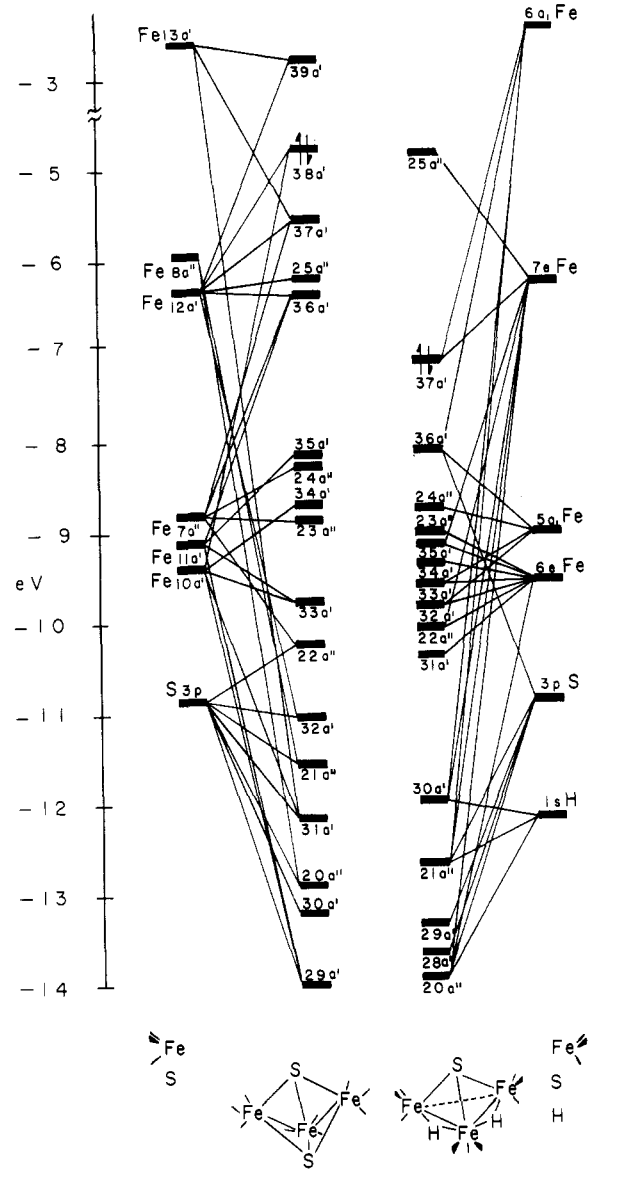

Figure 5. Molecular orbital bonding scheme comparing $S_2Fe_3(CO)_9$ with $SH_2Fe_3(CO)_9$. The energy values were obtained from a Fenske–Hall calculation. Connectivity lines indicate the principal contributions to each molecular orbital.

content. The M–H–M MO's are close to those of S–M in energy, and in $SH_2Fe_3(CO)_9$ the M–H–M a″ component mixes with the S–M a″ component to produce 20a″ and 21a″.

The fragment analysis for $SHFe_2Co(CO)_9$ formation indicates the importance of $M(CO)_3$ (M = Fe, Co) 7e and $6a_1$ orbitals. The free neutral fragments have orbital populations of $6e^{4.0}5a_1{}^{2.0}7e^{3.0}6a_1{}^{0.0}$ and $6e^{4.0}5a_1{}^{2.0}7e^{2.0}6a_1{}^{0.0}$ for $Co(CO)_3$ and $Fe(CO)_3$, respectively. The final cluster's populations for the $Co(CO)_3$ and $Fe(CO)_3$ fragments are $6e^{4.0}5a_1{}^{1.9}7e^{2.6}6a_1{}^{0.4}$ and $6e^{3.9}5a_1{}^{1.9}7e^{1.6}6a_1{}^{0.4}$, respectively. The H and S atoms absorb the excess electron density and have gross charges of 0.14– and 0.15–, respectively. The fragment analysis for $SH_2Fe_3(CO)_9$ formation is almost identical with that for $SHFe_2Co(CO)_9$. The H's and S bear overall negative charges of 0.14– and 0.16–, respectively.

$SH_2Fe_3(CO)_9$ and $S_2Fe_3(CO)_9$. The MO diagrams for $SH_2Fe_3(CO)_9$ and $S_2Fe_3(CO)_9$ are shown in Figure 5. The $SH_2Fe_3(CO)_9$ molecule was described above. For $S_2Fe_3(CO)_9$ the $Fe(CO)_3$ fragments were retained in their C_s symmetry. The $S_2Fe_3(CO)_9$ cluster formation will be presented in terms of the O_h t_{2g}-like (10a′, 11a′, and 7a″), the O_h e_g-like (12a′ and 8a″), 13a′, and two S atoms' 3p orbitals. The HOMO

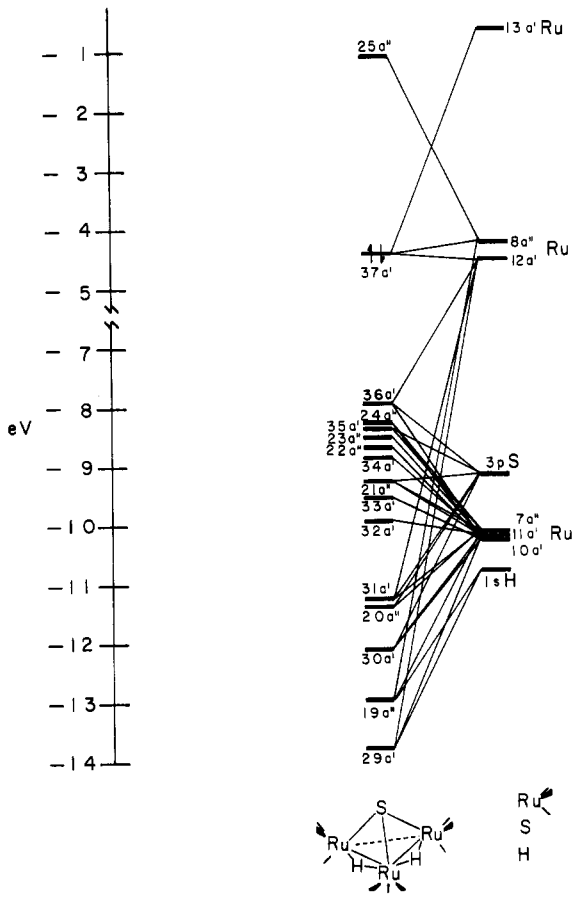

Figure 6. Molecular orbital bonding scheme for $SH_2Ru_3(CO)_9$. The energy values were obtained from a Fenske–Hall calculation. Connectivity lines indicate the principal contributions to each molecular orbital.

(38a′) and three orbitals directly under it are a mixture of t_{2g}- and e_g-like orbitals which form the two M–M bonds. The next group of orbitals are pure t_{2g}-like in character. The geometries of the CO's are rotated such that the two S atoms are equivalent. This creates a mixing of Fe e_g- and t_{2g}-like orbitals with S. This, coupled with the presence of two different Fe formal oxidation states, results in a broad energy range for the Fe and Fe–S MO's.

The fragment analysis for $S_2Fe_3(CO)_9$ is slightly complex. The $Fe(CO)_3$ fragment bonded to the other two Fe atoms will be designated as Fe*. In the free neutral fragments the orbital populations are $10a'^{2.0}11a'^{2.0}7a''^{2.0}12a'^{1.0}8a''^{1.0}13a'^{0.0}$. The final cluster's populations are $10a'^{2.0}11a'^{1.8}7a''^{1.8}12a'^{1.3}8a''^{0.7}13a'^{0.6}$ and $10a'^{2.0}11a'^{2.0}7a''^{2.0}12a'^{1.0}8a''^{0.7}13a'^{0.3}$ for $Fe^*(CO)_3$ and $Fe(CO)_3$, respectively.

$SH_2Ru_3(CO)_9$. The molecular orbital diagram for $SH_2Ru_3(CO)_9$ is shown in Figure 6. The $Ru(CO)_3$ fragments in the cluster were retained in their C_s symmetry geometry. The 10a′, 11a′, and 7a″ orbitals are the t_{2g}-like orbitals. The next two orbitals (12a′ and 8a″) correspond to the e_g-like orbitals. In the neutral fragment, 12a′ and 8a″ each contain one electron. The 13a′ orbital is the $Ru(CO)_3$ LUMO. The most important fragment orbitals for the formation of the cluster have their atomic character listed in Table V.

In forming the cluster, the $Ru(CO)_3$ fragments' e_g-like orbitals form only one M–M bonding orbital, the HOMO. The next group of orbitals are a mixture of $Ru(CO)_3$ t_{2g}-like orbitals destabilized by S 3p interactions. At lower energy 31a′, 20a″, and 30a′ correspond to the main Ru–S bonding MO's. These MO's include contributions from both the t_{2g}- and the e_g-like $Ru(CO)_3$ orbitals. The 19a″ and 29a′ orbitals represent Ru–H–Ru interactions. Although the major interaction of the H is with e_g-like orbitals, the M–H–M MO's are further stabilized by some interaction with t_{2g}-like orbitals. The fragment orbital composition of the $SH_2Ru_3(CO)_9$ molecular orbitals is listed in Table VI.

Table V. Atomic Composition of $Ru(CO)_3$ Fragments

	% atomic composition				
orbital	4d	5s	5p	CO 5σ	CO 2π
13a′ (LUMO)	12	22	32		33
8a″	45		32	6	16
12a′	49		28	6	16
7a″	81				19
11a′	78				20
10a′	77				22

Table VI. Molecular Composition of $SH_2Ru_3(CO)_9$

	% fragment composition							
orbital	13a′	8a″	12a′	7a″	11a′	10a′	H	S
25a″ (LUMO)		94	2					
37a′ (HOMO)	14	55	29					
36a′			14		3	52		27
24a″			4	69	2	17		5
35a′			9	73		4		10
23a″				7	88	4		
22a″		4		14	9	70		
34a′					94	4		
21a″		1	11	65		2		19
33a′			3	4	3	79		7
32a′	2	2			78	8	4	3
31a′	7	2	10	19		1		59
20a″	7	8	3	28			4	46
30a′	8				18	25	4	43
19a″	2	18	7	13		4	44	1
29a′	2	3	13			15	50	3

In terms of the $Ru(CO)_3$ fragment analysis, it is clear that most of the net cluster bonding involves the fragments' 12a′, 8a″, and 13a′ orbitals. In the free neutral $Ru(CO)_3$ fragments the orbital populations are $10a'^{2.0}11a'^{2.0}7a''^{2.0}12a'^{1.0}8a''^{1.0}13a'^{0.0}$. The $Ru(CO)_3$ fragment bonded to both H atoms will be designated as Ru*. The fragment orbital populations in the cluster are $10a'^{2.0}11a'^{2.0}7a''^{2.0}12a'^{0.8}8a''^{0.8}13a'^{0.4}$ and $10a''^{2.0}11a'^{2.0}7a''^{2.0}12a'^{0.7}8a''^{0.5}13a'^{0.3}$ for Ru and Ru*, respectively. The difference in the $Ru^*(CO)_3$ fragment's population is primarily due to the electron-withdrawing ability of the two H's.

Molecular Orbital Calculations: "Naked" Clusters. In the "naked" cluster approach, one begins with the tetranuclear clusters SCo_3, $SH_{n-1}Co_{3-n}Fe_n$ (n = 1–3) and considers how nine CO's perturb the "naked" cluster in forming the molecular clusters. The "naked" clusters may also serve as discrete models for metal–sulfide interactions on clean transition-metal surfaces.

The atomic composition of the "naked" SCo_3 cluster is shown on the left side of Figure 7. The LUMO is mostly Co 3d, stabilized by Co 4s and destablized by S 3p. The HOMO is pure Co 3d. The next 12 orbitals, designated by the rectangle labeled M–M, are predominantly Co–Co interactions. The MO labeled S represents the S 3p orbital perpendicular to the metal plane, a S–Co_3 σ-like bond. The two MO's labeled M–S designate S–Co_3 π-like interactions, which utilize the S 3p orbitals that are parallel to the Co_3 plane. Upon removal of one cluster electron by the exchange of one Co for an Fe the HOMO becomes mainly Fe in character. The other 11 orbitals within the M–M-labeled rectangle are Co–Co and Co–Fe bonding. The S–M interactions remain essentially unchanged.

The introduction of M–H–M interactions decreases the number of M–M bonding orbitals. In $SHFe_2Co$ the HOMO is almost pure Fe 3d. The next 10 orbitals in the M–M-labeled

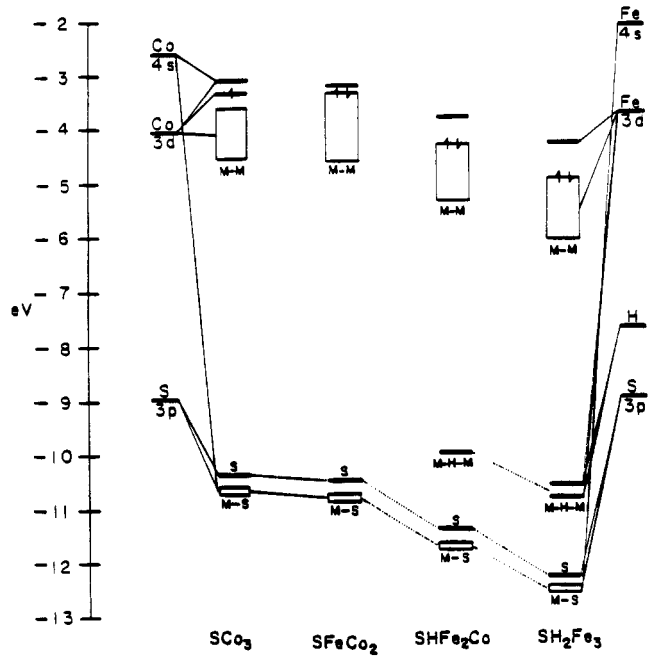

Figure 7. Molecular orbital bonding scheme for the "naked" clusters. The energy values were obtained from a Fenske–Hall calculation.

rectangle consists of 3 orbitals dominated by Co 3d and 7 orbitals dominated by Fe 3d atomic orbitals. The MO labeled M–H–M contains H (70%) and Fe 3d (22%). In the SH_2Fe_3 "naked" cluster, the introduction of another H has removed another high-energy M–M orbital, which increases the energy gap between the HOMO and the LUMO. The two orbitals labeled as M–H–M are composed of H (74% and 64%) and Fe 3d (predominantly the Fe attached to both H atoms). The S–M orbitals are similar but become progressively more stable as the H's are added to the cluster.

Addition of the nine carbonyls to the "naked" cluster lowers the eigenvalues as CO 2π stabilizes the metals' low oxidation state by accepting electron density. This interaction stabilizes some M–M antibonding orbitals while the carbonyl 5σ orbital destabilizes some M–M bonding orbitals. As shown by a comparison of Tables VII and VIII, there results an overall

Table VII. 3d Overlap Populations for Sulfide "Naked" Clusters

"naked" clusters	Mulliken overlap populations[a]					
	M–M	M–M*	S–M	S–M*	H–M	H–M*
SCo_3	0.013		0.052			
$SFeCo_2$	0.017	0.023	0.047	0.068		
$SHFe_2Co$	0.010	0.023	0.074	0.049	0.052	
SH_2Fe_3	0.027	0.008	0.075	0.075	0.056	0.056

[a] M* is the unique metal in every case.

reduction in M–M bonding when the nine carbonyls bond to the "naked" cluster.

Molecular Orbital Plots. In order to better understand the bonding in sulfide nonacarbonyl clusters, orbital plots have been made of the important M–M, M–S, and M–H–M bonding orbitals. Three planes have been plotted in order to delineate the interactions within a single orbital. One plane contains the metal basal plane. A second plane, perpendicular to the metal basal plane, contains a M atom, a S atom, and the center of the "tetrahedron". Since this plane slices through the interior of the cluster, it will be referred to as the interior plane. The third plane contains the other two M atoms, a S atom, and H atoms. This M_2S face plane is opposite the M atom in the interior plane. The solid contours and dashed contours represent positive and negative values of the wave function, respectively.

We will limit our MO-plot discussion to $SCo_3(CO)_9$ and $SH_2Ru_3(CO)_9$. The selection of $SCo_3(CO)_9$ is due to both its high molecular symmetry and structural resemblance to the isoelectronic series $SH_{n-1}Co_{3-n}Fe_n(CO)_9$ (n = 1–3). The $SH_2Ru_3(CO)_9$ complex will be used to illustrate the M–H–M interactions within the sulfide cluster series.

The contour plots of the $SCo_3(CO)_9$ MO's which are involved in the Co basal plane are shown in Figure 8. The HOMO, $8a_2$, shows the antibonding Co–Co interactions. From the cluster point of view, the remaining MO's shown in Figure 8 are all Co–Co bonding. The net cluster bonding arises primarily from $14a_1$ and 20e, which originate from the interaction of the $Co(CO)_3$ fragments' e_g-like orbitals, 7e.

The most important Co–S interactions in the interior plane are shown in Figure 9. A weak M–S σ^*-like bond is displayed in $13a_1$. The strong M–S π-like bond is shown in 16e. A σ-like

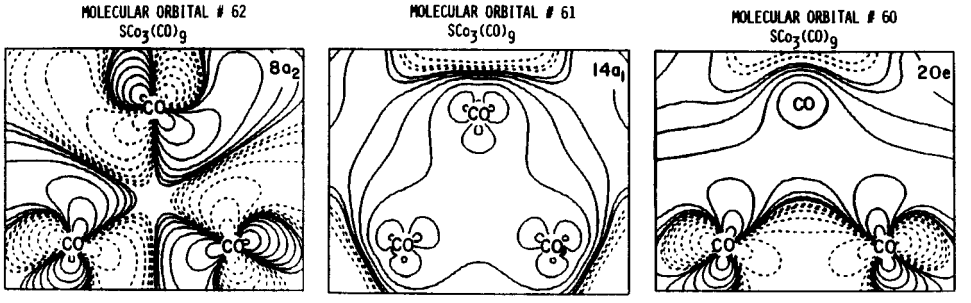

Figure 8. Orbital plots of $8a_2$, $14a_1$, and 20e in the cobalt-based plane of $SCo_3(CO)_9$. The lowest contour values are 2.44×10^{-4} e au^{-3}, and each succeeding contour differs from the previous one by a factor of 2.0.

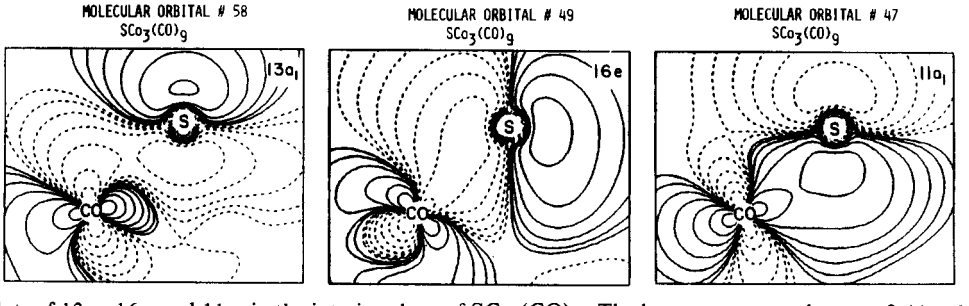

Figure 9. Orbital plots of $13a_1$, 16e, and $11a_1$ in the interior plane of $SCo_3(CO)_9$. The lowest contour values are 2.44×10^{-4} e au^{-3}, and each succeeding contour differs from the previous one by a factor of 2.0.

Table VIII. Mulliken Overlap Populations for the Sulfide Carbonyl Clusters[a]

	Mulliken overlap populations								
cluster	d-d	d-X	13a′-13a′	e_g-e_g	e_g-t_{2g}	t_{2g}-t_{2g}	e_g-X	t_{2g}-X	13a′-X
$SCo_3(CO)_9$									
Co-Co	0.004			−0.085	−0.124	0.009			
Co-S		0.054					0.099	0.006	
$SFeCo_2(CO)_9$									
Co-Co	0.009			0.049	0.113				
Co-Fe	0.011			0.014	0.130				
Co-S		0.050					0.088	0.005	
Fe-S		0.067					0.117	0.007	
$SHFe_2Co(CO)_9$									
Fe-Fe	0.006			0.024	0.223	0.003			
Fe-Co				0.019	0.031	0.002			
Fe-H		0.041					0.116	0.023	
Fe-S		0.063					0.111	0.006	
Co-S		0.047					0.086	0.004	
$SH_2Fe_3(CO)_9$									
Fe-Fe*	0.006			0.006	0.266	0.001			
Fe-Fe	0.014			0.027	−0.019	0.005			
Fe*-H		0.042					0.124	0.022	
Fe-H		0.040					0.107	0.025	
Fe*-S		0.058					0.103	0.004	
Fe-S		0.061					0.105	0.005	
$SH_2Ru_3(CO)_9$									
Ru-Ru*	0.004		−0.001	0.008	−0.001	−0.005			
Ru-Ru	0.021		0.016	0.086	−0.001	−0.003			
Ru*-H		0.081					0.145	0.009	0.009
Ru-H		0.073					0.124	0.012	0.035
Ru*-S		0.062					0.129	−0.009	0.109
Ru-S		0.062					0.123	−0.008	0.096

[a] An asterisk denotes that the metal is the unique one.

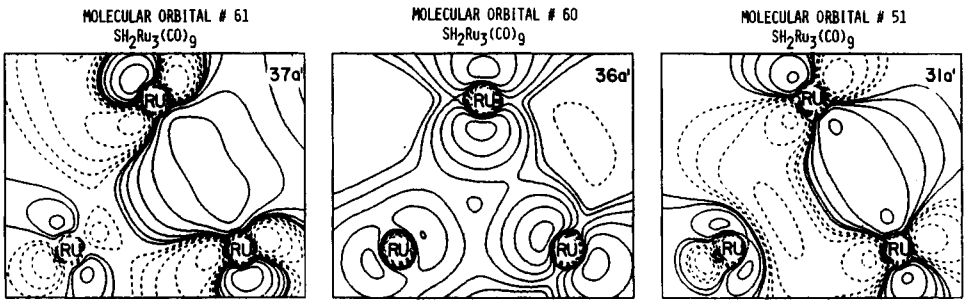

Figure 10. Orbital plots of 37a′, 36a′, and 31a′ in the basal plane of $SH_2Ru_3(CO)_9$. The lowest contour values are 2.44 × 10^{-4} e au^{-3}, and each succeeding contour differs from the previous one by a factor of 2.0.

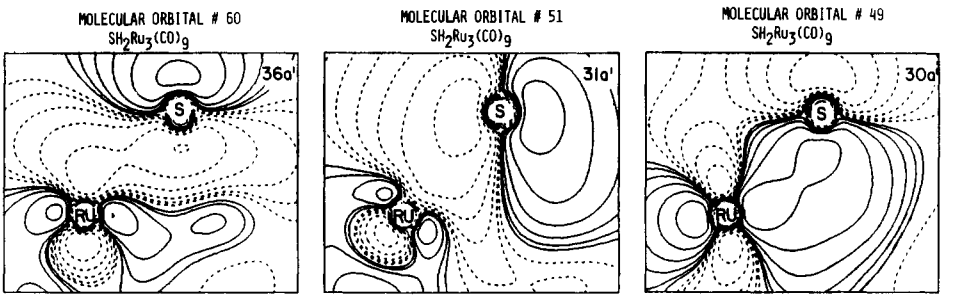

Figure 11. Orbital plots of 36a′, 31a′, and 30a′ in the interior plane of $SH_2Ru_3(CO)_9$. The lowest contour values are 2.44 × 10^{-4} e au^{-3}, and each succeeding contour differs from the previous one by a factor of 2.0.

bond between the S atom and the Co_3 base is represented in $11a_1$, but part of this is canceled in $13a_1$.

The Ru–Ru in-plane interactions are shown in Figure 10. Both 37a′ and 31a′ shown in Figure 10 are Ru–Ru bonding. These two orbitals originate from the $Ru(CO)_3$ fragments' e_g-like orbitals, 8a″ and 12a′. The net Ru–Ru bonding arises primarily from 37a′.

The important Ru–S bonding MO's are shown as interior planes in Figure 11. The 36a′ orbital cancels some to the Ru–S σ-like bonding present in 30a′. The 31a′ orbitals show a S–Ru π-like interaction, which is delocalized over all three Ru atoms.

Figure 12 shows one plane of the tetrahedral face containing the Ru–H–Ru interactions. In both of these MO's the Ru–H–Ru interaction looks like a three-center, two-electron bond with the maximum electron density located at the H positions. The orbitals (29a′ and 19a″) are more Ru–H than Ru–Ru bonding because more contours are crossed along the Ru–H internuclear axis than along the Ru–Ru axis.

Discussion

Photoelectron Spectra. In previous work the calculated one-electron orbital energies obtained from the Fenske–Hall method correlated reasonably well with the observed ionization

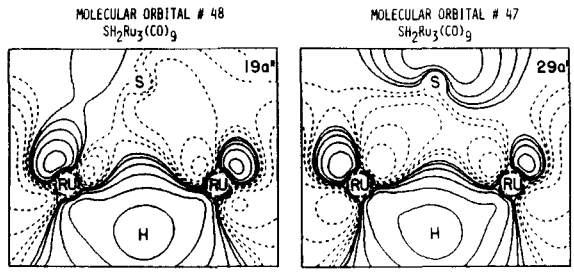

Figure 12. Orbital plots of 19a″ and 29a′ in the tetrahedral face plane of $SH_2Ru_3(CO)_9$. The lowest contour values are 2.44×10^{-4} e au^{-3}, and each succeeding contour differs from the previous one by a factor of 2.0.

energies in the PE spectra.[29] The partial PE spectra for $SCo_3(CO)_9$ and $SFeCo_2(CO)_9$[17] and $S_2Fe_3(CO)_9$[30] have already appeared. In low-energy PE spectra (Figure 1) for $SCo_3(CO)_9$, $SH_{n-1}Fe_nCo_{3-n}(CO)_9$ (n = 1–3), and $S_2Fe_3(CO)_9$, the first broad band can be reasonably assigned to ionizations that represent metal–metal bonds and metal–carbonyl π bonds. The metal–metal and metal–CO bonds are composed of the $M(CO)_3$ fragments' e_g- and t_{2g}-like orbitals, respectively. The shape of this lower energy band changes with the Co–Fe ratio. As the Fe character increases, the lower energy side of this band increases in peak intensity and, conversely, the higher energy portion of the first band decreases in peak intensity. This dramatic change in the shape of the band is not predicted by the calculations and may reflect a localization of the hole during the ionization process.[31] The first IE band of $S_2Fe_3(CO)_9$ is fairly broad due to the presence of two different Fe atoms. The diminutive band appearing before the first IE band in $SCo_3(CO)_9$ may be assigned to the unpaired electron in the Co–Co antibonding orbital.

The second band in these spectra is due to the M–S bonding interactions. The M–S interactions consist of $M(CO)_3$ fragments' e_g-like orbitals bonding with the S 3p orbitals. The M–S bond is composed of M–S σ-like and M–S π-like interactions. The M–S σ-like bond, **2** ($11a_1$), is partially canceled by a filled antibonding orbital ($13a_1$). The presence of an ionization due to the electrons in the latter orbital ($13a_1$) is in part responsible for the merging of the e_g-like and t_{2g}-like bands, which are clearly distinguished in the PE spectra of $Fe_3(CO)_{12}$. The net M–S σ-like overlap population is 0.011. The M–S π-like bonds, **3** (16e), are compsed of the remaining two S 3p atomic orbitals and the metal fragments' e_g-like orbitals. More of the net M–S bonding occurs through these π-like orbitals; the net M–S π-like overlap population is 0.039.

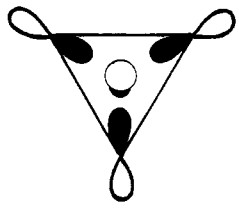

2

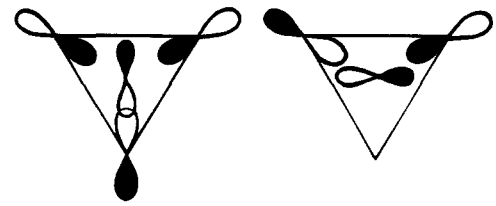

3

The S atom's 3s electron pair occurs at substantially higher IE and is not involved in M–S bonding. Formally, one may view the S as an S^{2-} ligand. When $M_3(CO)_9^{2+}$ is capped with S^{2-}, the S^{2-} ligand donates from both its σ and π orbitals. The net donation is indicated by Milliken populations. Each S 3p π-like orbital donates 0.70 electron, while the S 3p σ-like orbital donates only 0.35 electron.

The IE's for the M–H–M interactions are difficult to assign. Published results of other transition-metal complexes with bridging hydrogens list values ranging from 11.0 to 13.5 eV.[16b,32,33] Generally, the first-row transition-metal to H bands occur at lower IE's. The broad, intense Fe–S (σ and π) band hinders the exact location of the Fe–H–Fe ionizations. The Fe–H–Fe band(s) may occur either under the Fe–S band or may appear as the weak features between this band and the carbonyl 5σ and 1π ionizations, which begin at 13.9 eV. In $SH_2Fe_3(CO)_9$ the Fe–H–Fe bonds were calculated to be strongly mixed with the Fe–S interactions, as shown in Figures 4 and 5. This supports the assignment of the Fe–H–Fe IE's to the same region as the Fe–S IE band. However, there would then be no explanation for the weak features near 12.5 eV as the compounds appeared stable in the spectrometer.

In the PE spectra of $M_3(CO)_{12}$ and $SH_2M_3(CO)_9$ (M = Fe, Ru, Os), the clusters' bands change from a broad band in Fe to a manifold of closely spaced individual ionization peaks in Os. The fine structure observed in the IE bands of the Ru and Os sulfides (Figure 2) can be more quantitatively identified by comparison with the MO caculations (Figure 6). The first IE peak for $SH_2Ru_3(CO)_9$ and $SH_2Os_3(CO)_9$ PE spectra can be readily assigned to the 37a′, the M–M bond composed of e_g-like orbitals. The second low-intensity peak corresponds to the 36a′. This orbital is primarily t_{2g}-like but is destabilized by an antibonding interaction with S. This peak is more pronounced in the Os cluster because the t_{2g}-like orbitals are lower in energy and interact more strongly with S. This interaction between Os and S forces 35a′ into the leading edge of the t_{2g}-like band. The next strong band, which begins at about 9 eV, is due to closely spaced t_{2g}-like ionizations. The ones at lower IE are M–M antibonding, while the ones at higher IE are M–M bonding. Just below this IE manifold is another weak-intensity band which may be assigned to 33a′ and 32a′. These orbitals are t_{2g}-like and are strongly M–M bonding. Calculations suggest that the next IE manifold is mostly M–S bonding, mixed with some M–H–M interactions. The manifold can be readily assigned to 31a′, 20a″, and 30a′. Occurring at more stable energies will be two peaks, which can be assigned to M–H–M interactions, 19a″ and 29a′.

Nature of the Bonding. The calculations can be used to describe additional details of the electronic structure and bonding in the sulfide carbonyl clusters. They suggested there is little mixing between the t_{2g}- and e_g-like orbitals because the e_g–t_{2g} energy difference in the $M(CO)_3$ fragments is

(29) (a) Lichtenberger, D. L.; Fenske, R. F. *Inorg. Chem.* **1976**, *15*, 2015. (b) Lichtenberger, D. L.; Fenske, R. F. *J. Am. Chem. Soc.* **1976**, *98*, 50. (c) Block, T. F.; Fenske, R. F. *Ibid.* **1977**, *99*, 4321. (d) Hubbard, J. L.; Lichtenberger, D. L. *Inorg. Chem.* **1980**, *19*, 1388. (e) Morris-Sherwood, B. J.; Kolthammer, B. W. S.; Hall, M. B. *Ibid.* **1981**, *20*, 2771.

(30) Van Dam, H.; Stufkens, D. J.; Oskam, A. *Inorg. Chim. Acta* **1978**, *31*, L377.

(31) (a) Van Dam, H.; Stufkens, D. J.; Oskam, A.; Doran, M.; Hillier, I. H. *J. Electron Spectrosc. Relat. Phenom.* **1980**, *21*, 47. (b) Van Dam, H.; Louwen, J. N.; Oskam, A.; Doran, M.; Hiller, I. H. *Ibid.* **1980**, *21*, 57. (c) Cox, P. A.; Benard, M.; Beillard, A. *Chem. Phys. Lett.* **1982**, *87*, 159. (d) Newton, M. D. *Ibid.* **1982**, *90*, 297.

(32) (a) Green, J. C.; Seddon, E. A.; Mingos, D. M. P. *J. Chem. Soc., Chem. Commun.* **1979**, *94*. (b) Green, J. C.; Mingos, D. M. P.; Seddon, E. A. *J. Organomet. Chem.* **1980**, *185*, C20. (c) Wong, K. S.; Dutta, T. K.; Fehlner, T. P. *Ibid.* **1981**, *215*, C48. (d) Green, J. C.; Mingos, D. M. P.; Seddon, E. A. *Inorg. Chem.* **1981**, *20*, 2595. (e) Part 2: Sherwood, D. E., Jr.; Hall, M. B. *Ibid.* **1982**, *21*, 3458.

(33) DeKock, R. L.; Wong, K. S.; Fehlner, G. P. *Inorg. Chem.* **1982**, *21*, 3203.

Table IX. Atomic Charges for the Sulfide Nonacarbonyl Clusters[a]

cluster	atomic charges M	S	H
$SCo_3(CO)_9$			
Co	0.129-	0.130-	
$SFeCo_2(CO)_9$			
Co	0.141-	0.176-	
Fe	0.078+		
$SHFe_2Co(CO)_9$			
Co	0.134-	0.152-	0.141-
Fe	0.028-		
$SH_2Fe_3(CO)_9$			
Fe	0.046-	0.166-	0.141-
Fe*	0.062+		
$SH_2Ru_3(CO)_9$			
Ru	0.174+	0.497-	0.279-
Ru*	0.434+		
$S_2Fe_3(CO)_9$			
Fe(1)	0.005-	0.200-	
Fe(2)	0.075-		
Fe(3)	0.141+		

[a] An asterisk denotes that the metal is the unique one.

sufficiently large. The orbitals lying along the cluster's M-M internuclear axis are mainly derived from the e_g-like orbitals of the $M(CO)_3$ fragments.[34] These form a bonding set, which is totally occupied, and an antibonding unoccupied set. The M-H-M interactions are more intricate as suggested by the overlap populations in Table VIII. The M-M axis, bridged by H, has a decreased d-d overlap when compared to the nonbridged M-M interactions. The M(d)-H (M = Fe, Ru) overlap populations suggest that there are substantial disruptions of the M-M bond by a bridging H atom. The M-M bonds not bridged by H in these clusters are predominantly e_g-like in character. The loss of M-M e_g-like character to form M-H-M interactions is observed in both the calculations and the PE spectra. Interestingly the t_{2g}-like overlap populations go positive in the H-bridged FeCo clusters. It is this interaction, enhanced by a second H bridge, that is responsible for the short M-M bond in $H_2Os_3(CO)_{10}$.[32e]

Theoretically, the H atoms may interact with the metals directly by forming bonding and antibonding orbitals or indirectly by withdrawing charge.[35] The negative charge accumulated by H stabilizes the metal levels and results in a hydridic hydrogen. Recently, the geometrical[36] and theoretical[33] comparison between the isoelectronic $(\mu_3\text{-}CCH_3)Co_3(CO)_9$ and $(\mu_3\text{-}CCH_3)Fe_3(\mu\text{-}H)_3(CO)_9$ clusters suggests that the H atoms act like hydridic ligands. The gross charges for the H atoms in the Fe-H-Fe and Ru-H-Ru sulfides are 0.141- and 0.279-, respectively (Table IX). The S ligand also bears a negative charge (Table IX). As mentioned previously, the S 3p orbital directed toward the center of the cluster donates less electron density than those that are tangential. This important distinction arises because the inward-directed orbital interacts strongly with a t_{2g}-like metal orbital, which is sufficiently stabilized by the carbonyls that the M-S antibonding counterpart is also filled. Here again we see the participation of the t_{2g}-like orbitals, which are usually thought to be nonbonding.[37]

Acknowledgment is made to the Robert A. Welch Foundation (Grant A-648) and the National Science Foundation (Grant CHE 79-20993) for support of this work.

Registry No. 1, 22364-22-3; $SCo_3(CO)_9$, 35260-81-2; $SHFe_2Co(CO)_9$, 78547-58-7; $SH_2Fe_3(CO)_9$, 78547-62-3; $S_2Fe_3(CO)_9$, 22309-04-2; $SH_2Ru_3(CO)_9$, 32574-35-9; $SH_2OS_3(CO)_9$, 38979-82-7.

(34) Elian, M.; Hoffmann, R. *Inorg. Chem.* **1975**, *14*, 1058.

(35) (a) Hoffmann, R. *Acc. Chem. Res.* **1971**, *4*, 1. (b) Surjan, P. R.; Mayer, I.; Kertesz, M. *J. Chem. Phys.* **1982**, *77*, 2454.

(36) Wong, K. S.; Haller, K. J.; Dutta, T. K.; Chipman, D. M.; Fehlner, T. P. *Inorg. Chem.* **1982**, *21*, 3197.

(37) (a) Hoffmann, R. *Science (Washington, D.C.)* **1981**, *211*, 995 and references therein. (b) Hoffmann, R. *Angew. Chem., Int. Ed. Engl.* **1982**, *21*, 711 and references therein.

Contribution from the Division of Chemical and Physical Sciences, Deakin University, Waurn Ponds 3217, Victoria, Australia

Electrochemical-Electron Spin Resonance Investigation of Reactions of 17-Electron Iron Carbonyl Radical Cation Complexes

R. N. BAGCHI, A. M. BOND,* C. L. HEGGIE, T. L. HENDERSON, E. MOCELLIN, and R. A. SEIKEL

Received November 24, 1982

In situ electrochemical oxidation of $Fe(CO)_3(PPh_3)_2$ in dichloromethane in the cavity of an electron spin resonance (ESR) spectrometer, having variable-temperature capabilities and a microprocessor-based data acquisition system, enables the formation and decay of the 17-electron cation radical $[Fe(CO)_3(PPh_3)_2]^+$ to be studied. Electrolysis at platinum electrodes shows that $[Fe(CO)_3(PPh_3)_2]^+$ is relatively stable in noncoordinating solvents in the absence of oxygen and light. At silver and mercury electrodes, $[Fe(CO)_3(PPh_3)_2]^+$, while also being the stable product of electrolysis, is generated via silver and mercury intermediates, which are also light sensitive. $[Fe(CO)_3(PPh_3)_2]^+$ reacts with acetone (or acetonitrile) in a second-order process to produce transient solvent-substituted cation radical species that participate in a series of reactions to produce $Fe(CO)_3(PPh_3)_2$ and iron(II) compounds. These reactions appear to parallel those reported previously with anionic ligands. The reaction of $[Fe(CO)_3(PPh_3)_2]^+$ with PPh_3, $AsPh_3$, $SbPh_3$, $Fe(CO)_4PPh_3$, $Fe(CO)_3(AsPh_3)_2$, $Fe(CO)_4AsPh_3$, $Fe(CO)_3(SbPh_3)_2$, or $Fe(CO)_4SbPh_3$ in dichloromethane is stoichiometric and rapid, producing $Fe(CO)_3(PPh_3)_2$ and other species. Evidence for dimer formation as an intermediate is inferred from the ESR data with some of these reactions. Subsequent radical and molecular reactions lead to identification of $Fe(CO)_3(PPh_3)_2Cl$ at -35 °C, with chloride being obtained from the solvent dichloromethane.

The chemistry of zerovalent iron carbonyl moieties has been studied extensively.[1,2] The chemistry of iron(II) carbonyl complexes has also been examined in some depth.[1-4] The zerovalent complexes are predominantly five-coordinate, while

0020-1669/83/1322-3007$01.50/0